Single Image Defogging by Multiscale Depth Fusion

Yuan-Kai Wang, *Member, IEEE*, and Ching-Tang Fan, *Student Member, IEEE*

***Abstract*— Restoration of fog images is important for the deweathering issue in computer vision. The problem is ill-posed and can be regularized within a Bayesian context using a probabilistic fusion model. This paper presents a multiscale depth fusion (MDF) method for defog from a single image. A linear model representing the stochastic residual of nonlinear filtering is first proposed. Multiscale filtering results are probabilistically blended into a fused depth map based on the model. The fusion is formulated as an energy minimization problem that incorporates spatial Markov dependence. An inhomogeneous Laplacian–Markov random field for the multiscale fusion regularized with smoothing and edge-preserving constraints is developed. A nonconvex potential, adaptive truncated Laplacian, is devised to account for spatially variant characteristics such as edge and depth discontinuity. Defog is solved by an alternate optimization algorithm searching for solutions of depth map by minimizing the nonconvex potential in the random field. The MDF method is experimentally verified by real-world fog images including cluttered-depth scene that is challenging for defogging at finer details. The fog-free images are restored with improving contrast and vivid colors but without over-saturation. Quantitative assessment of image quality is applied to compare various defog methods. Experimental results demonstrate that the accurate estimation of depth map by the proposed edge-preserved multiscale fusion should recover high-quality images with sharp details.**

***Index Terms*— Dehaze, de-weathering, visibility restoration, contrast restoration, Markov random field.**

I. Introduction

OUTDOOR images are often suffered by suspended atmospheric particles such as haze, fog, smoke and mist that reduce the quality of the images taken in the scene. Visibility, contrast, and vividness of the scene are drastically degraded, which makes it difficult to distinguish objects. Enhancing the images acquired in poor weather conditions is called de-weathering and has been a very critical issue in applications such as aerial photography, driving assistance and visual surveillance. Defogging is a representative deweathering problem especially for removing the weather effect caused by suspended aerosol and water drops. The goal of defogging is to improve the contrast of the foggy images and restores the visibility of the scene.

Restoration of foggy scene from atmospheric scattering model [1] has been demonstrated to be successful. The atmospheric scattering model states the physical degradation process of foggy image as a linear combination of two components: attenuated scene reflectance and intensified atmospheric luminance, as shown in Fig. 1. The transmission medium is the suspended particles that influence the transmission of scene reflectance and atmospheric luminance. The scene reflectance is the albedo of the scene reflected by atmospheric luminance and is attenuated by the transmission medium. The atmospheric luminance is scattered by suspended particles intensified by the transmission medium and received by the observer as ambient arilight. The two components are additive due to the linear characteristic of light propagation. This physical process results in the degradation of both visibility and contrast.

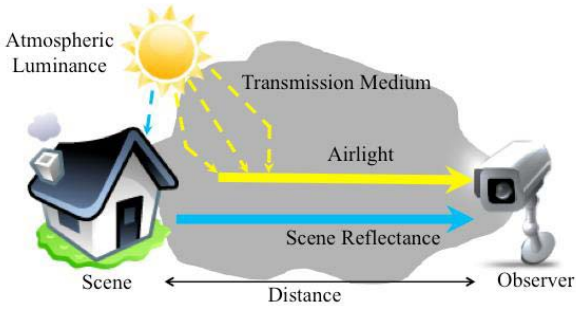

Fig. 1. The atmospheric scattering model of image degradation because of weathering.

Two critical factors affect the attenuation and intensification. The first is the atmospheric scattering coefficient of the transmission media that is deemed to the polarization characteristics of the particles and is usually assumed to be a constant in a static scene. The second factor is the distance between the scene and the observer. Longer distance induces more attenuation and intensification. While the depth is deeper, the effect is stronger and the foggy image loses more visibility and contrast. The two factors are combined into a single term called depth map in this paper. Estimating the depth map and airlight is therefore very crucial for the restoration of the scene reflectance.

Restoring true scene appearance from the single observation made in such bad weather conditions needs to estimate the depth map and airlight. The estimation remains a challenging task due to the inherent ambiguity that arises in the image degradation process. The ambiguity is an ill-posed problem: the number of known variables is less than the number of unknown variables. However, there are some clues or observations that can be considered as fog priors to resolve the ambiguity.

Manuscript received October 29, 2013; revised June 18, 2014; accepted August 25, 2014. Date of publication September 15, 2014; date of current version September 30, 2014. The associate editor coordinating the review of this manuscript and approving it for publication was Dr. Debargha Mukherjee.

The authors are with the Department of Electrical Engineering, Graduate Institute of Applied Science and Engineering, Fu Jen Catholic University, Taipei 24205, Taiwan (e-mail: ykwang@ieee.org; bevis@islab.tw).

Color versions of one or more of the figures in this paper are available online at http://ieeexplore.ieee.org.

Digital Object Identifier 10.1109/TIP.2014.2358076

Most existing endeavors are devoted to finding the fog priors from chromaticity constraints and contrast loss. Although the chromaticity prior was demonstrated to be a successful method for the estimation of depth map, the fog prior can be invalid when the scene object is similar to the airlight. Pixel-wise approach [2] may misestimate the depth map because white objects have similar chromaticity with haze. Patch-based approach such as the dark channel [3] alleviates the white object problem but induces halo effects. Fusion of the results from both approaches can compensate each other and obtain better estimation.

In this paper, we propose a multiscale depth fusion (MDF) method with local Markov regularization to recover fog images with only one single foggy image as input. The MDF method employs the Markov random field (MRF) to blend multi-level details of chromaticity priors. A stochastic relation between fog priors and depth map is first linearly modeled, and a new random field called inhomogeneous Laplacian-Markov random field (ILMRF) with the energy model incorporating the fog priors is proposed for the estimation of depth map. The ILMRF adaptively fuses the fog priors from multiscale filtering results according to local regularization. Two kinds of local regularization are considered. Smoothness of depth map is one of the local regularization because the change in depth of a scene is usually gradual and, hence, depth can be said to exhibit a local dependency. However, spatially localized physical transitions, such as abrupt changes in surface geometry surface composition or illumination, lead to discontinuities in intrinsic scene characteristics. Discontinuity-preservation is therefore another local regularization developed in the ILMRF. The energy function of ILMRF is an adaptive truncated Laplacian (ATL) that adapts to the local structure of the scene in order to provide better estimation of depth map.

The defog method first estimates the depth map and airlight, then applies the atmospheric scattering model to restore scene reflectance. The estimation of depth map is an iterated algorithm consisting of the alternate optimization of the two variables in the ATL potential: a line field variable for adaptive control and a base potential variable to regularize smoothness. Maximum likelihood scheme for the initialization and parameter estimation of the algorithm is applied to improve the efficiency of the iteration. The estimation of airlight utilizes the fused depth map with a smooth constraint to find fog-opaque regions that help compute more accurate atmospheric luminance.

This paper is organized as follows. We first briefly review existing methods for fog removal in Section II. In Section III, the fusion problem is formulated as a probabilistic linear model, and a new energy function considering fusion, smoothing and discontinuity-preserving is derived for the proposed ILMRF model. Algorithmic description of the MDF method is described in Section IV, that also presents the alternate optimization process for energy minimization of ILMRF, initialization of the iterated optimization process, and parameter estimation of ILMRF. Airlight estimation is also given here Section V shows experimental results as well as comparisons with some existing algorithms by quantitative measures of image quality. Finally, we conclude the paper and give future work in Section VI.

II. Related Works

Early works to the restoration of weather-degraded images treat the problem as yet another instance of image contrast enhancement [4]. However, these works can be regarded as a reduced case of the atmospheric scattering model that defogs image without considering the depth information [5], and is effective only for homogeneous haze. Polarization methods [6] remove haze by exploiting the difference of the polarization characteristics from the two images obtained by rotating a polarizing filter to different angles. These methods need a special hardware configuration that attaches the polarization filter to the camera.

A physical degradation process known as the atmospheric scattering model has been widely applied in many dehaze works [3]–[11]. The model is described as

$$I(x) = I_0(x)e^{-\beta d(x)} + \tilde{A}\big(1 - e^{-\beta d(x)}\big), \tag{1}$$

where $I(x)$ is the fog image, $\tilde{A}$ is the atmospheric luminance, and $I_0(x)$ is the scene reflectance without attenuation and also the fog-free image we desired. The distance between scene and observer at each pixel location $\boldsymbol{x}$ is given by $d(x)$, and the distance is proportional to the level of attenuation. The attenuation effect of transmission medium is described by $e^{-\beta d(x)}$, where β is the atmospheric scattering coefficient. The exponential term is called the depth map $D(\mathrm{x})$, i.e., $D(\mathrm{x}) = e^{-\beta d(x)}$. The airlight is expressed as the multiplication of atmospheric luminance and transmission media, i.e., $A(x) = \tilde{A}(1 - D(x))$. The atmospheric luminance is assumed to be a constant for many situations of bad weather particularly in daylight where the sky is usually overcast. The image degradation model is then simplified to be

$$I(x) = I_0(x)D(x) + A(x). \tag{2}$$

The scene reflectance is restored as follows:

$$I_0(x) = \frac{I(x) - A(x)}{D(x)} \tag{3}$$

given that the depth map and airlight are given.

The restoration has been identified as an ill-posed inverse problem [7] because two unknowns with one equation are used to solve the scene reflectance. Fog priors that are reasonable assumptions about the nature of the true scene reflectance makes the ill-posed problem into better posed and helps us obtain a better solution. A straightforward approach to obtain the fog priors is using additional information provided by human interaction, such as Kopf et al. [8] that introduces an interactive method by manually registering the haze image with existing geo-referenced 3D models. Narasimhan and Nayar [1], [5] make use of multiple haze images taken under different weather conditions to obtain the depth map. While the multiple image methods can significantly enhance visibility, unfortunately their requirements prevent them from delivering the results immediately and can be prohibitive in practical situations.

Single fog image contains sufficient information to directly determine the depth map, while single image defogging is still ill-posed and needs fog priors to resolve it [7]. Contrast and chromaticity are two fog priors usually applied for the estimation of depth map. The loss of contrast due to atmospheric scattering is an indication of scene depth [2], [5], [9]. While the visual loss of contrast can be a clue, this fog prior often gives wrong results for smooth albedo. Chromaticity prior [2], [3], [6], [7], [10], [11] has been demonstrated to be successful. In fog conditions, the appearance of an object becomes more similar to that of the fog as the distance between the camera and the object increases. Therefore, the colour dissimilarity between each pixel and the fog gives an indication about its depth. Chromaticity becomes a good bound on the possible scene depth at each pixel from the corresponding observed RGB color values [2].

Nonlinear filtering is an important approach to obtain depth map from chromaticity. There are two techniques: pixelwise and patchbased filtering. In [2] and [12] a nonlinear operation is applied pixel-wise and channel-wise to obtain finer estimates of depth map, and contextual constraints are followed to impose Markov regularization. The fine estimates prevent from the halos of path-based filtering at depth discontinuity, but needs more constraints to improve the accuracy. However, the indiscernibility of white objects and distant fog makes it difficult for accurate estimation of depth map. The depth of white objects could be near, but pixel-wise operations merely regard the pixels within white objects to be the appearance of fog. Patch-based filtering exploits the spatial correlation of image pixels for improvement. He et al. [3] imposes the dark channel constraints in local regions to obtain blocky estimates of the depth map. While the blocky estimate may resolve the white object problem, halo effect incurred by the estimate needs to be resolved.

Interestingly MRFs have been informally used to model the fog scene and improve the defog result in some works. [2] regularizes smoothness constraint in luminance field with natural image statistics of heavy-tail distribution on the gradient field. [7] assumes that the surface shading and the scene transmission are locally independent, and then uses a Gaussian MRF (GMRF) to smooth the scene transmission. [9] assumes the smoothness constraint in contrast field and regularizes it by a normalized Laplacian potential. [10] encodes geometry constraint into potentials and a Laplacian smooth term is applied to a homogeneous random field. [12] introduces a planar constraint for the defogging of the roadway area in vehicular applications and a homogeneous field is developed. However, homogeneous models with Gaussian potentials are not well suited to many image problems since they tend to oversmooth discontinuities, which is also true for defogging. A more efficient model should consider that only homogeneous regions are smooth and that edges must remain sharp. This motivates us to develop an inhomogeneous model that can adapt to the local structure of the image in order to provide a better estimation. A rigorous investigation of the preservation of sharp details in depth should be studied for defogging context.

III. Depth Fusion

Nonlinear filtering is usually applied to obtain a good bound on scene depth at each pixel from the corresponding observed RGB color values, because each pixel contains three measurements, the three channels of the observed foggy image, that may contribute to the depth estimation. The nonlinear filtering is a function over $I(x)$ defined as follows:

$$p(x) = f(I(x)), \tag{4}$$

where $f(\cdot)$ can be a maximum or minimum operator and $p(x)$ is called a prior map. The nonlinear operator can work on chromatic tristimulus and neighborhood pixels of $I(x)$. [2] adopts a maximum way channel-wise and pixel-wise because the farthest possible depth at each pixel is lower than the foggy intensity: $D(x) = (1/I_0)(I(x) - A(x)) < I(x) - A(x) < I(x) < \max_c I^c(x) = p(x)$, where $c \in \{R, G, B\}$ denotes color channel. The prior map becomes an upper bound of the depth map. The dark channel observation [3] says that the minimum intensity of an outdoor haze-free image is low and tends to be zero. A minimum operator is employed to obtain the prior map channel-wise and block-wise:

$$\begin{aligned} p(x) &= \min_c \min_{x' \in \Omega(x)} I^c(x') \\ &= \min_c \min_{x' \in \Omega(x)} (I_0(x') + A(x')) > \min_c \min_{x' \in \Omega(x)} A(x') \\ &> \max_{x' \in \Omega(x)} D(x'), \end{aligned}$$

where $\Omega(x)$ denotes a set of neighborhood pixels of x. This prior map is also an upper bound of the depth map. Both maximum and minimum operators play the same role for bounding. That is, only an approximate depth map can be obtained by the nonlinear filtering. Further regularization should be necessary to improve the result.

The block-based approach with the neighborhood systems $|\Omega| > 1$ deserves further exploration. Coarse scale of depth estimated with larger patch could prevent from the white object problem and obtain more correct depth information, but it also loses details and produces blocky and contouring effects on edge discontinuity. When patch size is small, the filtering result sustains more rich details. Unfortunately, the detail scale contains more incorrect depth information. An adaptive fusion approach to accommodate both advantages and reduce both drawbacks shall be beneficial for better estimation of depth map. We propose a Bayesian approach for the adaptive fusion of depth maps from multiple scales.

A. Problem Statement

We assume the prior maps that are depth maps $p(x)$ estimated from different scales are noisy and locally affine functions of a true depth map. Assume that there are m prior maps p_i, $i = 1, \ldots, m$. We want to produce a depth map D that is fused from p_i. Each prior p_i contains a good estimate of only part of D and is modeled in a probabilistic form relating p_i to D as follows

$$p(x) = H_i(x)D(x) + \varepsilon_i(x), \quad i = 1, \ldots, m, \tag{5}$$

where $\varepsilon_i(x)$ is the noise and $H_i(x)$ is called the prior weighting coefficient representing the percentage of the depth contributing to the ith prior map. A simplified model $p_i(x) = D(x) + \varepsilon_i(x)$ assuming $H_i(x)$ the same is adopted because we obtain all p_i from the same chromatic assumption. We choose Gaussian distribution to model $\varepsilon_i(x)$ with the variance $\sigma_i^2(x)$. The likelihood $P(p_i|D)$ accounting for the uncertainty of prior estimation and noise is therefore defined as follows:

$$P(p_i|D) = N\left(p_i|D, \sigma_i^2\right) \propto \exp\left\{-\frac{1}{\sigma_i^2}(p_i - D)^T(p_i - D)\right\}, \tag{6}$$

where $N(x|y, z)$ is a normal distribution of random variable x with mean y and variance z. We consider $\varepsilon_i(x)$ a non-stationary process. An adaptive method to estimate σ_i^2 is explained later.

Depth fusion is defined as the likelihood problem of $P(D|p_1, \ldots, p_m)$. We infer D by the maximum a posteriori (MAP) estimate

$$\begin{aligned}\tilde{D} &= \arg\max_D \{P(D|p_1, \ldots, p_m)\} \\ &= \arg\max_D \{P(p_1, \ldots, p_m|D)\, P(D)\} \\ &= \arg\max_D \{\ln P(p_1, \ldots, p_m|D) + \ln P(D)\}. \end{aligned} \tag{7}$$

Assume mutual independence of ε_i, we obtain

$$\begin{aligned}\ln P(p_1, \ldots, p_m|D) &= \ln \prod_i P(p_i|D) \\ &\propto -\sum\nolimits_i \frac{1}{\sigma_i^2}(p_i - D)^T(p_i - D). \end{aligned} \tag{8}$$

We assume that those priors have been gathered independently and our prior knowledge about D is assigned by a prior probability law $P(D)$ modeled by Gibbs distribution,

$$\ln P(D) = -\ln Z_D - U(D), \tag{9}$$

where Z_D is a partition function. Later we should give more attention to this prior knowledge $U(D)$. Then, substituting (8) and (9) into (7) and taking the constant term out, we formulate the depth inference problem with a proposed energy function $E(D)$:

$$\tilde{D} = \arg\max_D \{\exp(-E(D))\} = \arg\max_D \{E(D)\}, \tag{10}$$

where

$$E(D) = U(D) + \sum\nolimits_i \frac{1}{\sigma_i^2}(p_i - D)^T(p_i - D). \tag{11}$$

(10) and (11) formulate the depth fusion as an energy minimization problem. While a lot of energy minimization approaches have been proposed and can be applied to our formulation, the methods with regularized optimization considering spatial correlation are preferred. The fused depth map could be estimated pixel-by-pixel. However, it is very sensitive to prior noise. We can get better estimates of the depth map by utilizing spatial correlation since the changes of depth across the image tend to be smooth for the majority of the pixels. Motivated by the fact that the MRF model is currently the most effective way to describe the local behavior of both the intensity field and the discontinuity field, we develop an MRF model for the depth fusion problem.

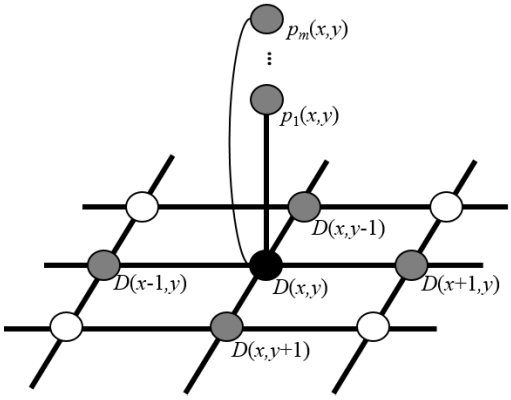

Fig. 2. Graphical representation of the proposed MRF model.

The first term in (11) is called the smoothing term that encodes local regularization for both smoothing and edge-preservation constraints. The second a data term accommodates the noisy effect of prior fusion and ensures the fidelity of the final fusion solution to the prior maps through the proposed stochastic model in (5). The smoothing term measures the extent to which the depth map is not piecewise smooth, while data term measures the disagreement between the depth map and prior maps. The MRF model that illustrates the stochastic relation of priors and spatial correlation is shown in Fig. 2. We consider three clique types in the four-neighborhood system associated with the singleton, vertical pairs, and horizontal pairs respectively.

The design of $U(D)$ is a critical issue. Regularization methods adopting standard Tikhonov theory [13] choose a quadratic potential function and make D smooth everywhere. This leads to poor results at object boundaries. Energy functions that do not have this problem are called edge preserving. These edge-preserving energy functions incorporate an adaptive interaction term giving a bound on the largest possible penalty. This avoids overpenalizing sharp jumps between the labels of neighboring pixels. Details are given in next subsection.

B. Adaptive Truncated Laplacian Potentials for Inhomogeneous Regularization

The depth map is represented as an undirected graph and adjacent nodes are connected to determine the depth of real scene. Let S be a set of sites in an image and $\Lambda \in \{0, 1, \ldots, L-1\}$ be the intensity space. We assume that $D(S) \in \Lambda^S$ follow MRF properties with the Gibbs potential $U(D) = \sum_{c \in S} U_c(D)$ that is defined by an autologistic function given by [14]. The smoothing term is defined as follows:

$$U(D) = \lambda \sum\nolimits_{x \in S} \sum\nolimits_{x' \in N(x)} V\left(D(x), D(x')\right), \tag{12}$$

where $D(x)$ is the latent label on pixel x and N is the set of adjacent pixels. N can be a different neighborhood system with Ω. $V(.)$ is the potential function that assigns a cost to

the label difference between the adjacent pixels x and x'. λ is a parameter to control the importance of smoothing term. Local regularization for smoothing and edge-preserving can be achieved by carefully defining a proper V.

Nonconvex potential functions instead of Gaussian are considered in this paper. Gaussian MRF (GMRF) adopts Gaussian potentials for smoothing and has been widely applied in many applications. However, the GMRF follows standard Tikhonov regularization theory, constitutes a homogeneous random field with a constant smoothing strategy, and hence induces over-smoothing especially for sudden intensity variation due to edges [15]. A scene depth can seldom be represented by homogeneous model because it is made up of different depth discontinuities both with objects and background. Edge-preserving smoothing is therefore an adaptive local regularization that adapts to the local structure of the depth prior yielding a less noising result in the homogeneous areas and also preserves sharp details for object boundaries. Spatially varying weights is a common approach for the adaptive smoothing with the result of sharp discontinuity that is advantageous for edge preserving [15]–[19].

Edge preservation considers that small gradients must be smoothed, while large gradients must be preserved. They have implicitly made the following assumption: A large value of the gradient corresponds to an edge while a small value of the gradient is an effect of noise. In the edge preservation models, the image is assumed to be generated by a two-level process, first introduced by Geman and Geman [20] and then formally called compound Gauss-Markov model [21]–[23]. The first level represents the correlations of adjacent pixels of the image. The second level contains a line process used to capture the image variations (edges). A general form of edge-preserving potential for two-level process model can be written as:

$$V\big(D(x), D(x')\big) = b\,(\Delta_x) \cdot \varphi\,(\Delta_x), \tag{13}$$

where $\Delta_x = D(x) - D(x')$ is the label difference, $b(\cdot)$ is a line field imposed as a spatially-varying weight function to adaptively control the strength of smoothing, and $\varphi(\cdot)$ is the potential of label difference. Here we call V an adaptive potential and φ a base potential. b is a nonnegative function and is usually a gradient field related to the variation structure (edge and texture) of D. Its role is to mark the location of discontinuities, and thus takes part in the preservation of edges. GMRF is a reduced form of (13) with b a constant and $\varphi(\Delta) = \Delta^2$ that adopts a homogeneous regularization strategy.

The base potential φ has been well studied. It can be a nonquadratic function that is required to be nonnegative, even and increasing. It has a common form $|\Delta|^p$, $p \in [1, 2]$. Existing results show that the Laplacian potential, $\varphi(\Delta) = |\Delta|$, tend to result in sharp discontinuity, which is advantageous to edge preserving [16], [24]. Another way to preserve edges is to use truncated potentials [16], [25]. Examples include the truncated quadratic $\varphi(\Delta) = \min(K, |\Delta|^2)$ and the truncated absolute distance $\varphi(\Delta) = \min(K, |\Delta|)$, where K is some constant. The truncated potentials encourage labelings of larger label difference that occurs at object's boundary and give these labelings a bound without increasing penalty.

The use of line fields was first introduced by Geman and Geman [20], who used a binary random field to model edges between intensity variables. Another effort uses a continuous line field to represent $b(\cdot)$. However, earlier efforts are not rigorous but rather heuristic, and a systematic framework derived from a rigorous model has been proposed by stochastic model or deterministic way. The stochastic model [18] assumes that the continuous line process is a Gaussian random process with spatially varying hyperparameters. Inhomogeneous GMRF (IGMRF) [15], [17], [26] adopts a deterministic way to represent the continuous line field. Both methods needs more parameters to control the degree of nonstationarity of the imposed image prior. Overparameterization of continuous line field methods induces heavy computational loading for the estimation of parameters. Binary line field is a good compromise for adaptiveness between model complexity and computational efficiency.

We model the depth map by an inhomogeneous random field, ILMRF, with an adaptive smoothing term that allows us to adjust amount of regularization locally. The ILMRF adopts an adaptive truncated Laplacian (ATL) potential with a binary line field. The base potential and the line field in ATL are defined by

$$\begin{aligned} \varphi\,(\Delta_x) &= \min\,(|\Delta_x|, V_{max}), \\ b\,(\Delta_x) &= 1 - S\,(|\Delta| - T), \end{aligned} \tag{14}$$

where $V_{\max}$ is an upper bound, S is a Heaviside step function, and T is a threshold. We use first-order neighborhood. The label difference becomes a vector, $\Delta_x = (\partial_H D(x), \partial_V D(x))$, where ∂ is a first-order derivative operator. The smoothing energy term is therefore defined as follows:

$$\begin{aligned} U(D) &= \lambda \sum\nolimits_{x \in S} b_H \varphi_H + \lambda \sum\nolimits_{x \in S} b_v \varphi_v \\ \text{where } b_i &= 1 - S\,(|\partial_i D(x)| - T), \\ \varphi_i &= \min\,(|\partial_i D(x)|, V_{max}), \quad i \in \{H, V\}. \end{aligned} \tag{15}$$

The horizontal line field element b_H aids in detecting a horizontal edge, while the vertical line field element b_V helps in detecting a vertical edge. We have chosen b_H and b_V to be binary variables over the line fields. The on-state of the line-process variable indicates that a discontinuity, in the form of a high gradient, is detected between neighboring points. Each turn-on of a line-process variable reduces the adaptive potential to be zero so as to keep discontinuities. This ATL potential is nonconvex and the energy minimization is solved by an iterative optimization approach combined with graph-cut methods.

IV. Defog Algorithm

A defog algorithm employing energy minimization to find the fused depth map and then restoring foggy images is presented in this section.

A. Energy Minimization

The introduced ATL potential enables us to compute the regularized depth map $\tilde{D}$ by minimizing the

Given D^0
$n \leftarrow 0$
Repeat
$b^{n+1} \leftarrow \arg\min_b E(D^n, b)$
$D^{n+1} \leftarrow \arg\min_D E(D, b^{n+1})$
$n \leftarrow n+1$
Until convergence.

Fig. 3. The alternate optimization of line fields and depth map for energy minimization of ILMRF.

following functional:

$$\tilde{D} = \arg\max_{D,b} E(D, b),$$

where

$$E(D,b) = \sum\nolimits_i \sigma_i^{-2} (p_i - D)^T (p_i - D) + \lambda \sum\nolimits_{x \in S} \{b_H \varphi_H + b_v \varphi_v\}. \quad (16)$$

b is a dummy variable representing both horizontal and vertical line fields. The minimization process has to simultaneously estimate both D and b, which is a very difficult task and computationally demanding. An important characteristic of the edge-preserving regularization is that the computation involves the minimization of nonconvex energy functionals, in contrast to the minimization of a quadratic potential function that a simple gradient method can quickly find the minimum [15], [17], [26]. Hence it needs costly optimization methods such as simulated annealing [20], [21] and Markov chain Monte Carlo [27], [28] in order to estimate the unknown depth by stochastic approach.

Alternate optimization methods, such as graduated nonconvexity [29], mean-field annealing [30] and ARTUR [24], are deterministic methods that demand less computation. They separate the simultaneous estimation into two successive steps: alternate minimizations on the line field b and then on the hidden label D. An iterative process of the alternate minimization has to be applied until convergence.

Fig. 3 gives the proposed alternate optimization method. At every step of the algorithm, new line fields are computed from the last depth estimate and then taken into account for the computation of the new depth estimate. Since D^n is fixed at step $n+1$, b^{n+1} is simply computed using (14). The successive minimization over D with fixed b^{n+1} is still not easy because the truncated Laplacian function in $E(D,b^{n+1})$ is nonconvex. Truncated functions can be proved to be NP-hard to compute the exact minimum and need computationally expensive search for global optimization [25]. While it is NP-hard, the graph-cut method [19] provides an expansion-move algorithm that iteratively runs min-cut/max-flow algorithms on appropriate graph and efficiently finds a local minimum with respect to large moves. The algorithm finds a labeling extremely close to global solutions within a known factor. The expansion-move algorithm was shown to be applicable to any energy where V is a metric functional on the space of labels [31], [32]. The metric property of a V is defined such that $V(\alpha,\alpha) + V(\beta,\gamma) \leq V(\alpha,\gamma) + V(\beta,\alpha)$ is preserved for all labels α, β, and γ. Since the truncated Laplacian follows the metric property we can apply the graph-cut method to find an approximate solution of $E(D,b^{n+1})$.

The convergence of the sequence D^n can be proved to be valid even for the nonconvex potential because $(b^{n+1} - b^n) \to 0$ and $(D^{n+1} - D^n) \to 0$ as $n \to +\infty$. Theoretically, the iteration consisting of a sequential update of D and b should be carried out indefinitely; but, in practice, it is done a sufficient number of times to yield good.

In our algorithm, the noise variances σ_i^2 in (16) and (18) are unknown and a data-driven optimal estimation of σ_i^2 has to be developed. Because we assume that the noise in the fusion model is a Gaussian noise, it is straightforward to estimate the noise variance by the maximum likelihood criterion. It is given by

$$\left(\hat{\sigma}_i^2\right)^{n+1} = \arg\max P\left(p_i | D^n, \sigma_i^2\right) = \frac{1}{M} \left\| p_i - D^n \right\|^2, \quad (17)$$

where M is the number of pixels.

B. Initialization

The energy minimization process presented in Fig. 3 needs an initial estimate D^0 to start the iteration. Theoretically, the algorithm converges independent of the initial estimate. However, in practice, discretely selected initial estimates lead to better solutions in fewer iterative steps. The choice of initial solution determines the speed of convergence. Use of a close approximate to the solution as an initial estimate can speed up the optimization process.

We derive an initial estimate from a relaxed energy function with $U = 0$. The energy function in (16) is reduced to $E(D) = \sum_i \sigma_i^{-2} |p_i - D|^2$. We have an explicit expression obtained by putting $dE/dD = 0$:

$$D^0 = \frac{1}{\sum_i w_i} \left(\sum\nolimits_i w_i p_i \right) \text{ with } w_i = \frac{1}{\sigma_i^2}, \quad i = 1, \ldots, m. \quad (18)$$

The solution is rewritten with a weighted linear form:

$$D^0 = WP, \quad \text{where } P = [p_1, \ldots, p_m], \quad W = (A^T A)^{-1} A^T, \quad A = [w_1, \ldots, w_m]^T. \quad (19)$$

That is, the initial estimate is a weighted average of prior maps. However, this formulation provides a global weighting way. A local weighting scheme adaptively fuses prior maps by local variances $\sigma_i^2(x)$ is given as follows:

$$D^0(x) = W(x)P(x), \quad \text{where } P(x) = [p_1(x), \ldots, p_m(x)],$$
$$W(x) = \left(A^T(x)A(x)\right)^{-1} A^T(x), \; A(x) = [w_1(x), \ldots, w_m(x)]^T,$$
$$w_i(x) = \frac{1}{\sigma_i^2(x)}, \text{ where } \sigma_i^2 = \frac{1}{|N(x)| - 1} \sum_{x' \in N(x)} \left(I(x') - \bar{I}(x)\right)^2. \quad (20)$$

C. Airlight Estimation

The airlight function $A(\boldsymbol{x})$ is the multiplication of two factors: atmospheric luminance $\tilde{A}$ and the inverse of depth map. We can assume that a portion of the image contains pixels infinitely far away. The image points corresponding to

scene points at infinity $d(x) = \infty$ are regarded as the set of representative color vectors of atmospheric luminance and an average operation is applied to estimate the expected color vector of atmospheric luminance. The search of the infinity pixels that are called fog-opaque pixels is also critical for solving $A(\boldsymbol{x})$.

High-intensity assumption is commonly used for the search of fog-opaque pixels. White pixels that have the highest intensity values in the fog image are considered as atmospheric luminance, since these pixels may represent the scene points with no reflection, assuming to be at infinite distant. Color constancy methods such as white patch have been directly applied [1], [2], [9], [10]. Fattal [7] applies the principle of uncorrelation to search within small windows of constant albedo for the white pixels that yield the least correlation. However, over-saturation may happen when white objects appear with the highest intensities.

In this paper we assume the fog-opaque pixels exist not only in the deepest region of the depth map, but also in smooth regions of fog images, because the fog-opaque region exhibits atmospheric luminance and conceals textured appearance of the scene. All pixels in the fog-opaque region are averaged to obtain the color vector of the atmospheric luminance $\tilde{A} = \{\tilde{A}^r, \tilde{A}^g, \tilde{A}^b\}$:

$$\tilde{A}^c = \frac{1}{|R|} \sum\nolimits_{x \in R} I^c(x), \quad c \in \{\mathrm{r}, \mathrm{g}, \mathrm{b}\}, \tag{21}$$

where R is the fog-opaque region and $|R|$ is the number of pixels in R. R is decided by the following criteria:

$$R = \left\{ x | \tilde{D}(x) = \arg\min_{l} h(l) \right\}, \tag{22}$$

$$h(l) = \sum\nolimits_{x} E(x) \cdot \delta(\tilde{D}(x) = l), \tag{23}$$

where $h(l)$ is the histogram of smoothness with respect to the depth label l estimated by ILMRF, $E(x)$ is an edge image indicating the smoothness of a region, and $\delta(\cdot)$ is a Kronecker delta function.

D. The Algorithm

The proposed MDF method to automatically restore a foggy image is summarized as follows. First, we use an existing nonlinear filtering method to estimate the depth maps with different scales. The depth maps obtained this way are not sufficiently accurate to solve the defog problem and are called prior maps. We apply these prior maps to the proposed ILMRF and minimize the energy function (16) by the alternate optimization to get the regularized result that is the major contribution of this paper and is given in the second and third steps of the algorithm. Atmospheric luminance is then computed from the fused depth map combined with a smoothness constraint. Finally the inverse of the atmospheric scattering model is utilized to restore the scene reflectance. The following give an algorithmic description of the MDF method:

1) Filter the foggy image nonlinearly with multiple scales;
2) Estimate the initial depth estimate D^0 by (20);
3) Regularize depth map $\tilde{D}$ by the alternate optimization presented in Fig. 2;
4) Compute atmospheric luminance $\tilde{A}$ by (21);
5) Restore the scene reflectance I_0 by (3).

E. Time Complexity Analysis

Time complexity of the proposed method is analyzed with respect to the number of pixels M and the number of labels N. Steps (1), (2), (4) and (5) have $O(M)$ complexity. The major cost of computations of the MDF takes place on step (3) due to graph-cut computation of the ILMRF for depth labeling over 2D grids. It takes $O(M^3N)$ [19], but an improvement up to $O(M^3)$ can be done by [33]. The alternate optimization procedure iteratively applies the MDF algorithm with a fixed number of times, which can be considered as a constant term in the complexity analysis. Therefore, The time complexity of the proposed method is $O(M^3)$.

V. Experimental Results

Experimental results are qualitatively and quantitatively compared with many existing algorithms to demonstrate the effectiveness of our method. Our experiments was conducted on benchmark fog images collected from a variety of sources [2], [3], [7]–[9], [11], [12]. These images exhibits diverse challenges of the defog problem. We classify them into two categories according to scene complexity: smooth depth and cluttered depth. The fog images in smooth-depth category usually contain a small sky region and an overlook view. White objects such as clouds, white landmarks or white buildings are prone to incur wrong depth estimation. Cluttered-depth fog images exhibit complex depth discontinuity that happens due to occlusion of foreground objects.

Two parameters of the proposed MDF method are fixed in our experiments: $m = 2$ and $T = 128$. The applied nonlinear filter is minimum operator. The sizes of small and large patches in the filter, $|\Omega|$, are adjusted depending on image size, fog size, and object details. Sizes of small patches range from 1 to 5, and those of large patches from 15 to 35. The regularization parameter λ remains to be a variable to regularize the smoothness of depth fusion. The effectiveness of edge-preserved depth fusion of the ILMRF model is first given in the followings. We then compares the proposed MDF method with various defog algorithms. More results and our matlab code can be downloaded from the Web.[1]

A. Edge-Preserved Depth Fusion

The ILMRF plays an important role for edge preservation in depth domain. Edge-preserved depth estimates help MDF recover better results. Here we give some examples to show the strength of edge-preserved depth fusion.

A synthetic image experiment is given in Fig. 4. This example simulates a scene with two albedos and corresponding depth discontinuity. Given a synthetic foggy image shown in Fig. 4(c), the proposed MDF recovers an excellent result shown in Fig. 4(d) with the edge-preserved depth map obtained by ILMRF, as shown in Fig. 4(e). The results shown in Figs. 4(e) and 4(f) are obtained by [3] and [7]. These results

[1] http://rr.ykwang.tw/

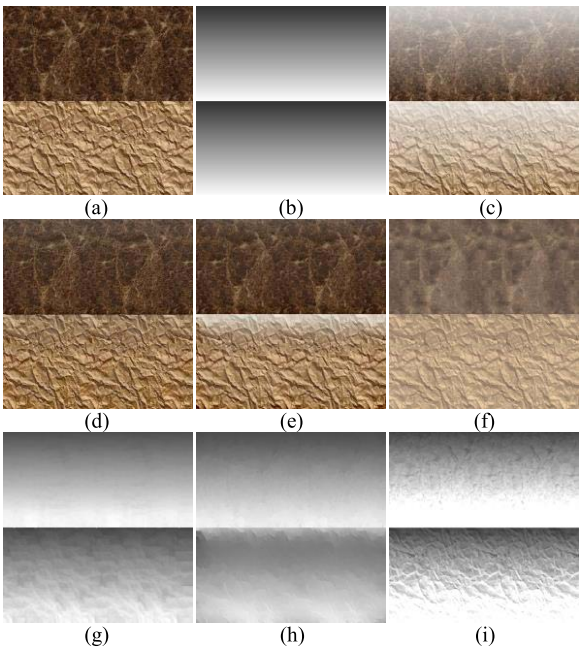

Fig. 4. Synthetic experiment. (a) Synthetic two-albedo image. (b) Synthetic transmission. (c) Synthetic foggy image. Recovered images (d) by MDF, (e) by [3], and (f) by [7], respectively. Estimated transmissions (g) by ILMRF, (h) by [3], and (i) by [7], respectively.

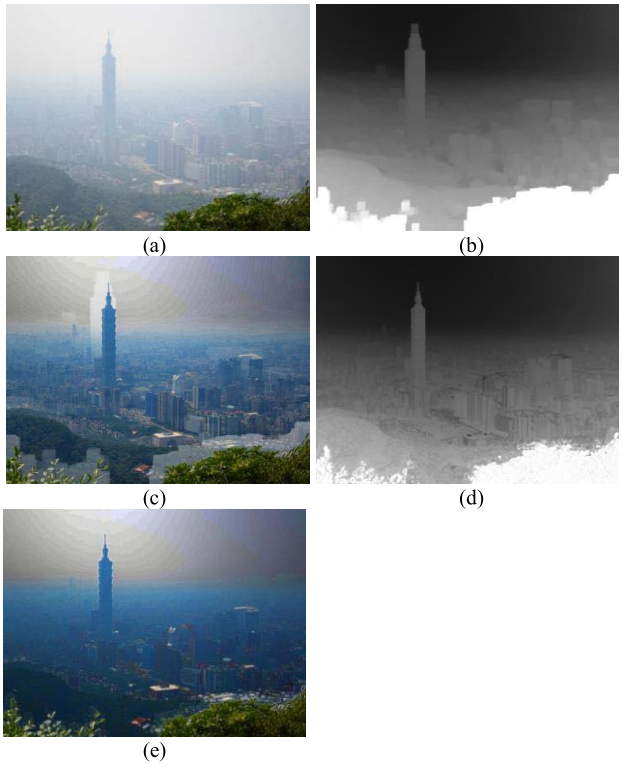

Fig. 5. Halo effect of defogging incurred by block-based nonlinear filtering. (a) A fog image, (b) the depth map estimated by 19×19 dark channel prior, (c) defog result. (d) Depth map by ILMRF. (e) Recovered results by MDF.

have artifacts because the estimates of depth maps by both methods are not good enough, especially in the boundary of depth discontinuity. Fig. 5 illustrates the halo effect produced by block-based nonlinear filtering. Fig. 5(a) shows a foggy image of Taipei downtown. The depth map estimated by dark channel prior of 19×19 blocks is given in Fig. 5(b), and the defog image restored by [3] in Fig. 5(c). Lower values (black pixels) in the depth image indicate deeper depth. The halo effect shown in Fig. 5(c) is induced by incorrect depth estimation around the Taipei 101 building, where a dilated shape of the building is seen in Fig. 5(b). This problem cannot be easily solved by soft matting or edge-preserving filtering. Fig. 5(d) gives a more accurate depth map calculated by ILMRF. Restored result by MDF without halo effect is given in Fig. 5(e).

An illustration of depth fusion is shown in Fig. 6. Fig. 6(a) is a surveillance image with dense haze with severe loss of visibility, contrast, and vividness. White vehicles and landmarks in the image are challenging to chromaticity prior. Figs. 6(b) and 6(c) give two prior maps estimated with a small patch and a large patch. None are satisfied estimates. The depth-prior pixels of the white vehicles and landmarks in Fig. 6(b) have lower values that represent deep estimates, but they are incorrect estimates. The white object problem is alleviated in Fig. 6(c), but blocky estimates incur halo effect. Fusion of the two prior maps with the global weighting scheme given in (19), $D = wp_1 + (1 - w)p_2$, with different w is shown in Figs. 6(d)(e)(f). It is observed that larger w favors small-block estimation, and small w large-block estimation. These results reveal the flaw of global weighting scheme. Adaptive weighting by (20) is shown in Fig. 6(g). Both overestimation and blocky-estimation problems are alleviated. While a small area within the white-vehicle region is still incorrectly estimated, it is successfully rectified in the refined depth map shown in Fig. 6(h). A smooth and accurate depth map is obtained by imposing edge-preserving and smoothing constraints with Markov regularization.

Fig. 7 compares the depth estimates obtained by He et al. [3], Fattal [7] and ILMRF with respect to smooth- and cluttered-depth scenes. It shows a cluttered-depth example with leaves in front of the scene. Fig. 7(c) shows blocky results although the dark channel prior has been enhanced by soft matting. The proposed ILMRF gets sharp depth edges consistent with the fog scene in both examples. By blending priors of different scales, our approach isolates fine edges between different depth objects with much finer detail.

Fig. 8 illustrates the importance of edge-preservation for defogging with another cluttered-depth example. Depth estimation without edge preservation in depth domain produces bad recovery image having fog-opaque pixels around foreground objects. The challenge in Fig. 8(a) is the depth discontinuity caused by the green leaves in front of the scene. Fig. 8(b) shows the depth map obtained by guided filtering [34] with dark channel estimation, and Fig. 8(c) the depth map by ILMRF. The guided filter is an edge-preserving filter that can be applied to improve dark channel results, while carefully tuning a lot of parameters is necessary. The depth discontinuity of the scene is not preserved in Fig. 8(b), which induces veil effect in Fig. 8(d). Our approach more accurately estimates the depth variation of the scene at finer granularity around foreground objects, such as the leaves on the left side. The results shown in Figs. 8(c) and 8(e) demonstrate the accuracy

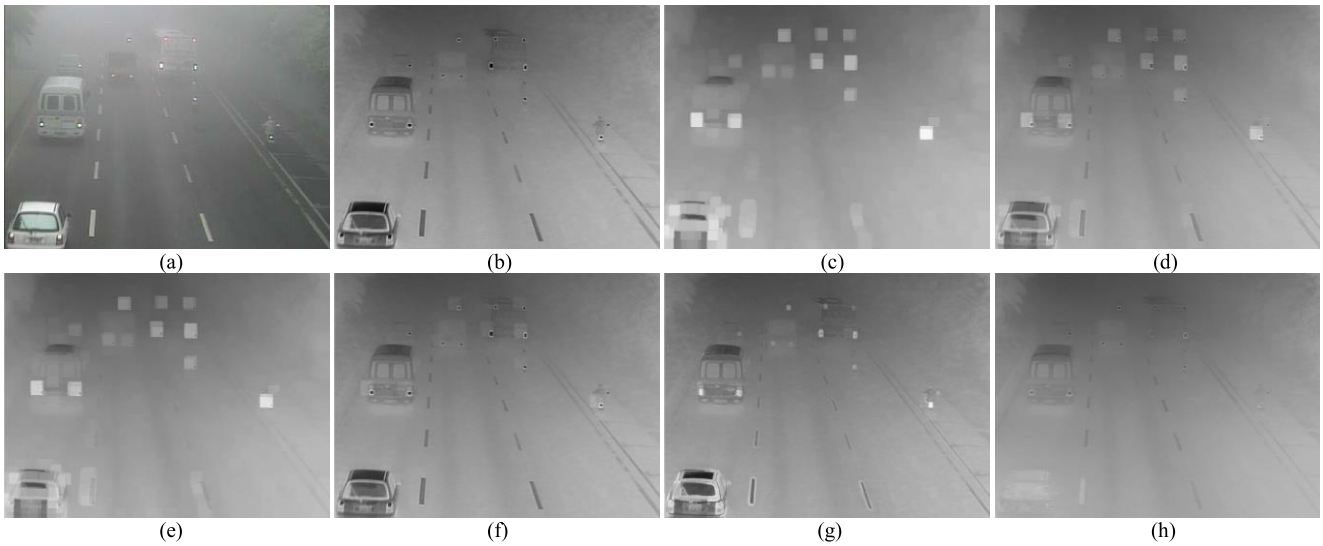

Fig. 6. Reduction of halo effect by depth fusion. (a) A foggy image, (b) the depth map estimated by pixelwise piror, i.e., dark channel prior with $|\Omega| = 1$, (c) the depth map estimated by dark channel prior with $|\Omega| = 19$. The fusion results by global weighting scheme with (d) $w = 1/2$, (e) $w = 1/5$, and (f) $w = 4/5$. (g) is the initialized depth map $\tilde{D}$ obtained by adaptive weighting scheme. (h) is the regularized depth map obtained by ILMRF.

Fig. 7. Comparison of depth estimates for a cluttered-depth image. (a) A foggy forest image. Depth maps obtained by (b) Fattal's method, (c) He's method, and (d) ILMRF.

Fig. 8. Comparison of edge-preservation between guided filter and ILMRF. (a) A foggy image of depth discontinuity caused by foregrounds. Refined depth maps obtained by (b) guided filter and (c) ILMRF. Restored results obtained by (d) guided filter and (e) ILMRF.

of the edge-preserving regularization enabled with ILMRF. Note that sharpness is not necessary enhanced in Fig. 8(e), since the ILMRF is applied only in depth domain but not in image domain.

B. Defog Algorithm Comparison

The proposed MDF method was compared with existing algorithms, including Nishino et al. [2], He et al. [3], Fattal [7], Kopf et al. [8], Tan [9], Zhang et al. [11], and Tarel et al. [12]. Defogging results are compared with image qualities measured with one no-reference assessment method DIIVINE [35], and two full-reference assessment methods, structural similarity index (SSIM) [36] and peak signal-to-noise ratio (PSNR). DIIVINE assesses image quality blindly without the need of reference images. Its scores range from 0 to 100 and zero score means the best quality. For PSNR and SSIM measures we adopt foggy images as references, because no fog-free images exist in these benchmark data. Lower PSNR and SSIM scores imply greater dissimilarity between restored results and referenced foggy images, which means better quality. Therefore, for all the three measures lower scores indicate better defogging results.

Figs. 9(a) and 10(a) give two smooth-depth examples. Defogging results of five algorithms [3], [7]–[9], [12] are compared in these two examples. Fig. 9(a) is a foggy city

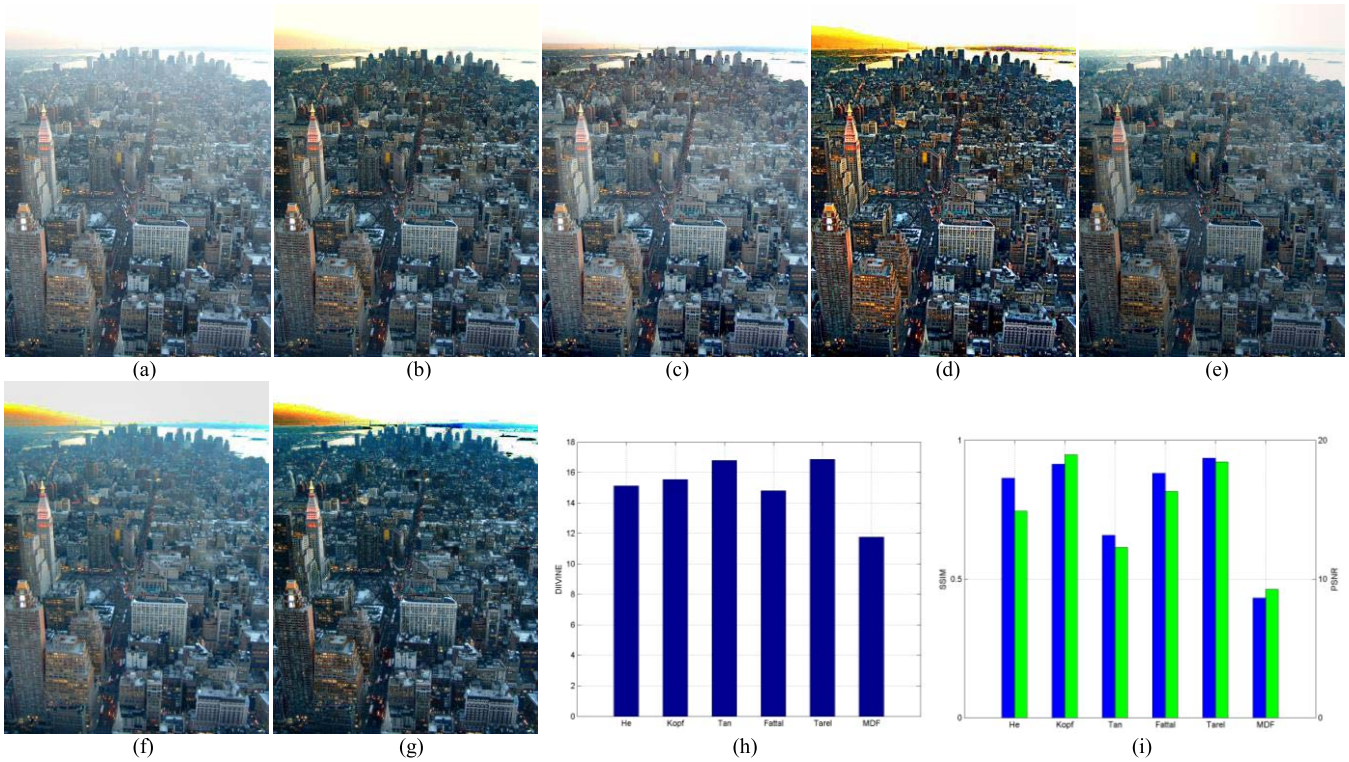

Fig. 9. Restoration of a city image with haze. (a) The observation image. Defogging results of (b) He, (c) Kopf, (d) Tan, (e) Fattal, (f) Tarel, and (g) MDF. Image qualities of defogging results are assessed by (h) DIIVINE, (i) SSIM and PSNR.

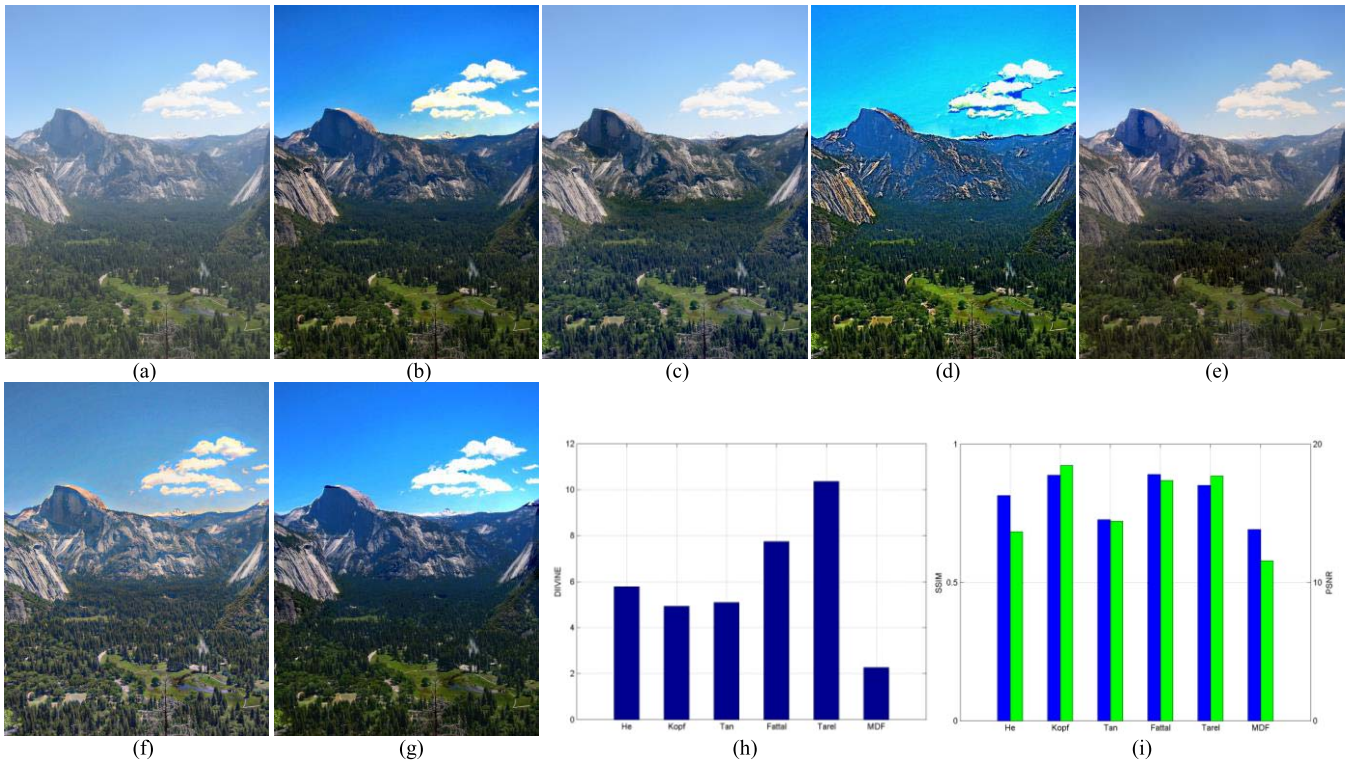

Fig. 10. Restoration of a natural scene with clouds and mists. (a) The observation image. Defogging results of (b) He, (c) Kopf, (d) Tan, (e) Fattal, (f) Tarel, and (g) MDF. Image qualities of defogging results are assessed by (h) DIIVINE, (i) SSIM and PSNR.

image with loss of visibility near the skyline. All the compared methods successfully improve visibility and local contrast of the scene, except that Tan's method show oversaturated colors and excessive contrast with increased noise. Our results exhibit greater consistency in colors besides the removal of haze. The two plots in Figs. 9(h) and 9(i)

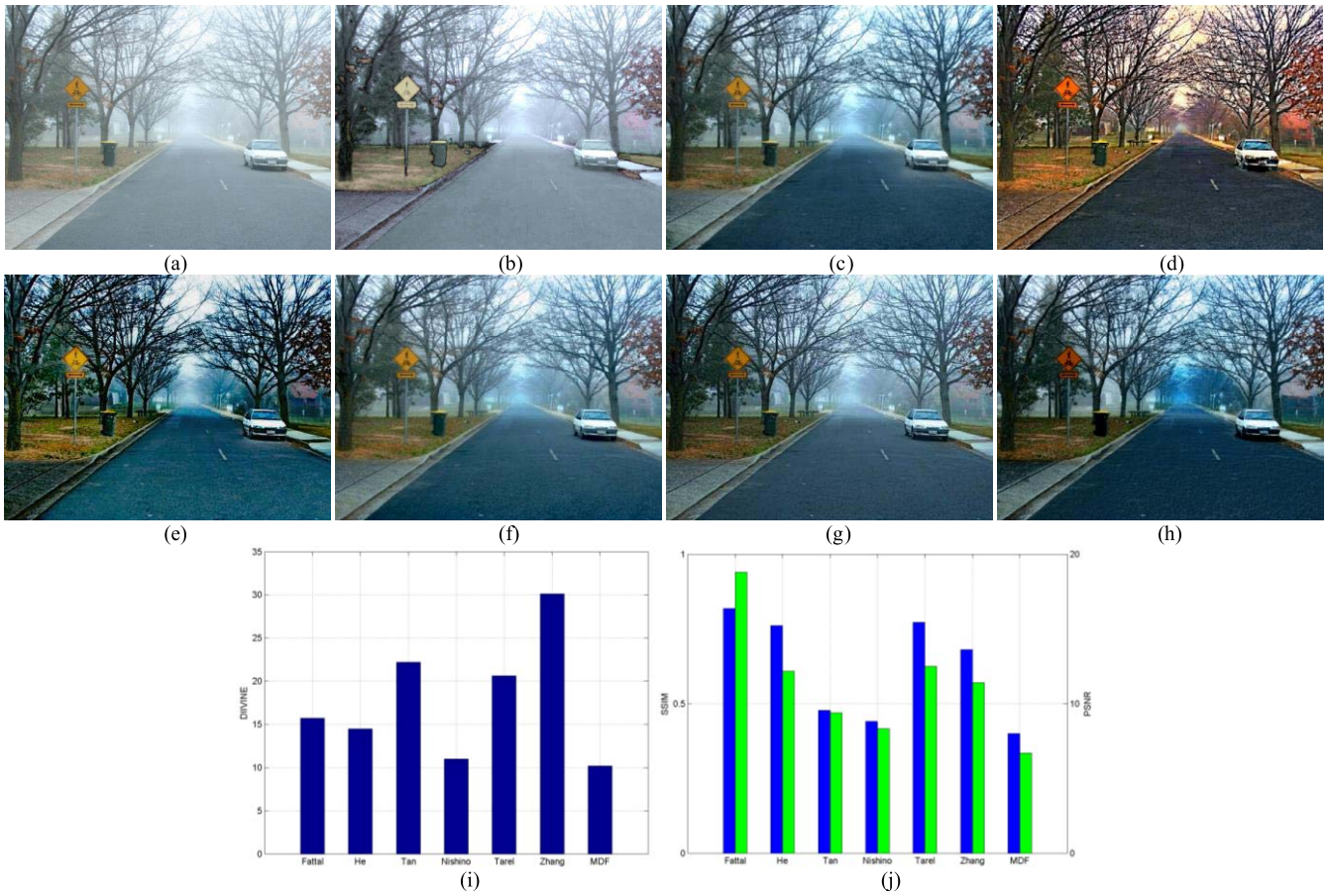

Fig. 11. Restoration of a dense-fog image with cluttered depths segmented by trees (a) The observation image. Defogging results of (b) Fattal, (c) He, (d) Tan, (e) Nishino, (f) Tarel, (g) Zhang, and (h) MDF. Image qualities of defogging results are assessed by (i) DIIVINE, (j) SSIM and PSNR.

validate these observations with objective measures considering balanced scoring among noise, structure similarity, and local contrast. The recovery of the scenes without sacrificing the fidelity of the colors is achieved by our method because the accurate estimation of the proposed atmospheric luminance method. Recovery of Fig. 10(a) is prone to contaminate the clouds and produces artifacts in mountains. Our method not only prevents from the contamination and artifacts, but also casts improved blue tints and local contrast. These results get better quantitative scores in DIIVINE, SSIM and PSNR.

Fig. 11 gives a cluttered-depth example. Results of seven algorithms [2], [3], [7]–[9], [11], [12] are compared. It uncovers a challenge in airlight estimation. The color vectors of atmospheric luminance reside at small regions fragmentally distributed among leaves or slender branches, which cannot be correctly estimated without very accurate depth estimates at finer granularity. Tan's method obtains over-saturated result due to wrong airlight estimation. Fattal's method fails to estimating depths. Nishino's method may have better contrast and sharp details, but increase noises. Our defog results achieve not only vivid colors and better perception, but also the best objective measurement, demonstrating the success of depth accuracy and the effectiveness of constraining both smoothness and edge-preservation.

VI. Conclusion

We have presented a multiscale depth fusion method for single image defogging. The proposed ILMRF embeds the fusion scheme into adaptive Markov regularization to achieve better estimation of depth map. The ATL potential constitutes an inhomogeneous field that adaptively regularizes the depth map for the preservation of depth discontinuity. The non-convexity of ATL is solved by an alternate optimization approach. Two adaptive weighting schemes, one for the line field in ATL and another for initial fusion of multiple scales, are devised to automate the complicated regularization process. The fusion of multiple scales was visually illustrated in a set of experimental results with better scene depths in alleviating both the halo effect and white object problem. Assessment of defog image quality also validates better contrast and sharpness of the proposed method. The edge-preserved fusion approach not only achieves accurate depth estimates but also restores fog-free images with sharp details at finer granularity. Several future works can be drawn from experimental results. Contrast could be another kind of fused priors to be applied to the ILMRF framework. An appropriate quality measure considering the characteristics of fog images will help the rigorous study of defogging. Fusion of more than two scales could also be investigated, while time efficiency should be considered.

REFERENCES

[1] S. G. Narasimhan and S. K. Nayar, "Vision and the atmosphere," *Int. J. Comput. Vis.*, vol. 48, no. 3, pp. 233–254, Jul. 2002.

[2] K. Nishino, L. Kratz, and S. Lombardi, "Bayesian defogging," *Int. J. Comput. Vis.*, vol. 98, no. 3, pp. 263–278, Nov. 2011.

[3] K. He, J. Sun, and X. Tang, "Single image haze removal using dark channel prior," *IEEE Trans. Pattern Anal. Mach. Intell.*, vol. 33, no. 12, pp. 2341–2353, Dec. 2011.

[4] J. P. Oakley and H. Bu, "Correction of simple contrast loss in color images," *IEEE Trans. Image Process.*, vol. 16, no. 2, pp. 511–522, Feb. 2007.

[5] S. G. Narasimhan and S. K. Nayar, "Contrast restoration of weather degraded images," *IEEE Trans. Pattern Anal. Mach. Intell.*, vol. 25, no. 6, pp. 713–724, Jun. 2003.

[6] Y. Y. Schechner, S. G. Narasimhan, and S. K. Nayar, "Polarization-based vision through haze," *Appl. Opt.*, vol. 42, no. 3, pp. 511–525, 2003.

[7] R. Fattal, "Single image dehazing," *ACM Trans. Graph.*, vol. 27, no. 3, pp. 1–72, Aug. 2008.

[8] J. Kopf *et al.*, "Deep photo: Model-based photograph enhancement and viewing," *ACM Trans. Graph.*, vol. 27, no. 5, pp. 1–116, Dec. 2008.

[9] R. T. Tan, "Visibility in bad weather from a single image," in *Proc. IEEE Conf. Comput. Vis. Pattern Recognit.*, Jun. 2008, pp. 1–8.

[10] P. Carr and R. Hartley, "Improved single image dehazing using geometry," in *Proc. Digit. Image Comput. Techn. Appl.*, Dec. 2009, pp. 103–110.

[11] J. Zhang, L. Li, G. Yang, Y. Zhang, and J. Sun, "Local albedo-insensitive single image dehazing," *Vis. Comput.*, vol. 26, nos. 6–8, pp. 761–768, Apr. 2010.

[12] L. Caraffa and J.-P. Tarel, "Markov random field model for single image defogging," in *Proc. IEEE Intell. Veh. Symp.*, Jun. 2013, pp. 994–999.

[13] T. Poggio, V. Torre, and C. Koch, "Computational vision and regularization theory," *Nature*, vol. 317, no. 26, pp. 314–319, Sep. 1985.

[14] S. Z. Li, *Markov Random Field Modeling in Image Analysis*. New York, NY, USA: Springer-Verlag, 2001.

[15] M. Joshi and A. Jalobeanu, "MAP estimation for multiresolution fusion in remotely sensed images using an IGMRF prior model," *IEEE Trans. Geosci. Remote Sens.*, vol. 48, no. 3, pp. 1245–1255, Mar. 2010.

[16] S. S. Saquib, C. A. Bouman, and K. Sauer, "ML parameter estimation for Markov random fields with applications to Bayesian tomography," *IEEE Trans. Image Process.*, vol. 7, no. 7, pp. 1029–1044, Jul. 1998.

[17] P. P. Gajjar and M. V. Joshi, "New learning based super-resolution: Use of DWT and IGMRF prior," *IEEE Trans. Image Process.*, vol. 19, no. 5, pp. 1201–1213, May 2010.

[18] G. K. Chantas, N. P. Galatsanos, and A. C. Likas, "Bayesian restoration using a new nonstationary edge-preserving image prior," *IEEE Trans. Image Process.*, vol. 15, no. 10, pp. 2987–2997, Oct. 2006.

[19] Y. Boykov and V. Kolmogorov, "An experimental comparison of min-cut/max-flow algorithms for energy minimization in vision," *IEEE Trans. Pattern Anal. Mach. Intell.*, vol. 26, no. 9, pp. 1124–1137, Sep. 2004.

[20] S. Geman and D. Geman, "Stochastic relaxation, Gibbs distributions, and the Bayesian restoration of images," *IEEE Trans. Pattern Anal. Mach. Intell.*, vol. PAMI-6, no. 6, pp. 721–741, Nov. 1984.

[21] F.-C. Jeng and J. W. Woods, "Compound Gauss–Markov random fields for image estimation," *IEEE Trans. Signal Process.*, vol. 39, no. 3, pp. 683–697, Mar. 1991.

[22] J. Zhang, "Parameter reduction for the compound Gauss–Markov model," *IEEE Trans. Image Process.*, vol. 4, no. 3, pp. 382–386, Mar. 1995.

[23] R. Molina, A. K. Katsaggelos, J. Mateos, A. Hermoso, and C. A. Segall, "Restoration of severely blurred high range images using stochastic and deterministic relaxation algorithms in compound Gauss–Markov random fields," *Pattern Recognit.*, vol. 33, no. 4, pp. 555–571, 2000.

[24] P. Charbonnier, L. Blanc-Féraud, G. Aubert, and M. Barlaud, "Deterministic edge-preserving regularization in computed imaging," *IEEE Trans. Image Process.*, vol. 6, no. 2, pp. 298–311, Feb. 1997.

[25] Y. Boykov, O. Veksler, and R. Zabih, "Fast approximate energy minimization via graph cuts," *IEEE Trans. Pattern Anal. Mach. Intell.*, vol. 23, no. 11, pp. 1222–1239, Nov. 2001.

[26] A. Jalobeanu, L. Blanc-Féraud, and J. Zerubia, "An adaptive Gaussian model for satellite image deblurring," *IEEE Trans. Image Process.*, vol. 13, no. 4, pp. 613–621, Apr. 2004.

[27] R. G. Aykroyd, "Bayesian estimation for homogeneous and inhomogeneous Gaussian random fields," *IEEE Trans. Pattern Anal. Mach. Intell.*, vol. 20, no. 5, pp. 533–539, May 1998.

[28] A. Jalobeanu, L. Blanc-Féraud, and J. Zerubia, "Hyperparameter estimation for satellite image restoration using a MCMC maximum-likelihood method," *Pattern Recognit.*, vol. 35, no. 2, pp. 341–352, Feb. 2002.

[29] A. Blake and A. Zisserman, *Visual Reconstruction*. Cambridge, MA, USA: MIT Press, 1987.

[30] D. Geiger and F. Girosi, "Parallel and deterministic algorithms from MRFs: Surface reconstruction," *IEEE Trans. Pattern Anal. Mach. Intell.*, vol. 13, no. 5, pp. 401–412, May 1991.

[31] V. Kolmogorov and R. Zabin, "What energy functions can be minimized via graph cuts?" *IEEE Trans. Pattern Anal. Mach. Intell.*, vol. 26, no. 2, pp. 147–159, Feb. 2004.

[32] R. Szeliski *et al.*, "A comparative study of energy minimization methods for Markov random fields with smoothness-based priors," *IEEE Trans. Pattern Anal. Mach. Intell.*, vol. 30, no. 6, pp. 1068–1080, Jun. 2008.

[33] V. Lempitsky, C. Rother, and A. Blake, "LogCut—Efficient graph cut optimization for Markov random fields," in *Proc. IEEE 11th Int. Conf. Comput. Vis.*, Oct. 2007, pp. 1–8.

[34] K. He, J. Sun, and X. Tang, "Guided image filtering," *IEEE Trans. Pattern Anal. Mach. Intell.*, vol. 35, no. 6, pp. 1397–1409, Jun. 2013.

[35] A. K. Moorthy and A. C. Bovik, "Blind image quality assessment: From natural scene statistics to perceptual quality," *IEEE Trans. Image Process.*, vol. 20, no. 12, pp. 3350–3364, Dec. 2011.

[36] Z. Wang, A. C. Bovik, H. R. Sheikh, and E. P. Simoncelli, "Image quality assessment: From error visibility to structural similarity," *IEEE Trans. Image Process.*, vol. 13, no. 4, pp. 600–612, Apr. 2004.

Yuan-Kai Wang (M'01) received the B.S. degree in electrical engineering and the Ph.D. degree in computer science and information engineering from National Central University, Zhongli, Taiwan, in 1990 and 1995, respectively. He was a Post-Doctoral Fellow with the Institute of Information Science of Academia Sinica, Taipei, Taiwan, from 1995 to 1999. In 1999, he joined the Department of Electrical Engineering at Fu Jen University, Taipei, as an Associate Professor.

He has been the Chair and a Program Committee Member of many international conferences, and a reviewer of many journals and IEEE transactions. His research interests include computer vision, pattern recognition, and machine learning. He studied applications of the above methods on video surveillance, face recognition, biometrics, and robotic vision. He is currently interested in machine learning and video analysis for visual surveillance, embedded computer vision, human–computer interface, robotics, and health care.

Ching-Tang Fan (S'14) received the B.S. degree in electrical engineering from Fu Jen Catholic University, Taipei, Taiwan, in 2008, where he is currently pursuing the Ph.D. degree in computer science with the Graduate Institute of Applied Science and Engineering. His research interests include pattern recognition, image processing, and embedded computer vision, with a special focus on their application to video surveillance system integration.